



NRL/MR/7130--06-8965

PAVAD B Design and Experimental Results Report

PETER C. HERDIC

SFA, Inc.

Crofton, MD

BRIAN H. HOUSTON

ROBERT D. CORSARO

Physical Acoustics Branch

Acoustics Division

June 30, 2006

REPORT DOCUMENTATION PAGE

Form Approved
OMB No. 0704-0188

Public reporting burden for this collection of information is estimated to average 1 hour per response, including the time for reviewing instructions, searching existing data sources, gathering and maintaining the data needed, and completing and reviewing this collection of information. Send comments regarding this burden estimate or any other aspect of this collection of information, including suggestions for reducing this burden to Department of Defense, Washington Headquarters Services, Directorate for Information Operations and Reports (0704-0188), 1215 Jefferson Davis Highway, Suite 1204, Arlington, VA 22202-4302. Respondents should be aware that notwithstanding any other provision of law, no person shall be subject to any penalty for failing to comply with a collection of information if it does not display a currently valid OMB control number. **PLEASE DO NOT RETURN YOUR FORM TO THE ABOVE ADDRESS.**

1. REPORT DATE (DD-MM-YYYY) 30-06-2006		2. REPORT TYPE Memorandum Report		3. DATES COVERED (From - To)	
4. TITLE AND SUBTITLE PAVAD B Design and Experimental Results Report				5a. CONTRACT NUMBER	
				5b. GRANT NUMBER	
				5c. PROGRAM ELEMENT NUMBER	
6. AUTHOR(S) Peter C. Herdic,* Brian H. Houston, and Robert D. Corsaro				5d. PROJECT NUMBER	
				5e. TASK NUMBER	
				5f. WORK UNIT NUMBER	
7. PERFORMING ORGANIZATION NAME(S) AND ADDRESS(ES) Naval Research Laboratory, Code 7130 4555 Overlook Avenue, SW Washington, DC 20375-5320				8. PERFORMING ORGANIZATION REPORT NUMBER NRL/MR/7130--06-8965	
9. SPONSORING / MONITORING AGENCY NAME(S) AND ADDRESS(ES) KAPL, Inc. Knolls Atomic Power Laboratory P.O. Box 1072 Schenectady, NY 12301-1072				10. SPONSOR / MONITOR'S ACRONYM(S)	
				11. SPONSOR / MONITOR'S REPORT NUMBER(S)	
12. DISTRIBUTION / AVAILABILITY STATEMENT Approved for public release; distribution is unlimited.					
13. SUPPLEMENTARY NOTES *SFA, Incorporated, Crofton, MD 21114					
14. ABSTRACT The application and experimental results are presented for the Passive and Advanced Vibro-Acoustic Treatments Demonstration, Part B (PAVAD-B) conducted at the Laboratory for Structural Acoustics, Naval Research Laboratory (NRL) during the winter and spring of 2001-2002. The goal of this demonstration is to utilize the most advanced treatments developed in the first part of the program (PAVAD-A), improve their design, and apply them to the Sponsor Supplied Structure. In the initial PAVAD-A study, advanced treatments were applied to an idealized simple supported plate to evaluate the noise reduction performance and optimize the treatment designs. Nearfield Acoustic Holography (NAH) measurements of the untreated Sponsor Supplied Structure were also made and previously reported. These holography data illustrate the structural response and provide a means to determine the optimized PAVAD-B treatment locations. The performance of the improved PAVAD-B advanced treatments is evaluated using these same NAH techniques on the Sponsor Supplied Structure and reported in this document.					
15. SUBJECT TERMS Control of acoustics					
16. SECURITY CLASSIFICATION OF:			17. LIMITATION OF ABSTRACT	18. NUMBER OF PAGES	19a. NAME OF RESPONSIBLE PERSON
a. REPORT	b. ABSTRACT	c. THIS PAGE			Brian H. Houston
Unclassified	Unclassified	Unclassified	UL	22	19b. TELEPHONE NUMBER (include area code) (202) 404-3840

CONTENTS

I. INTRODUCTION.....	1
II. BRIEF REVIEW OF PAVAD-A	1
III. PAVAD-B EXPERIMENTAL CONFIGURATION	2
A. Nearfield Acoustic Holography (NAH) And Measurement Issues	3
B. Advanced Treatment Design And Configuration	3
C. Control Laws And Configuration	8
IV. ADVANCED TREATMENTS PERFORMANCE.....	11
A. Broadband Untreated/Treated (System-Off) Performance	11
B. Tonal Untreated/Treated(System-Off)/Treated(System-On) Performance.....	14
V. CONCLUSIONS	19
REFERENCES:	19
APPENDIX A.....	20

PAVAD B DESIGN AND EXPERIMENTAL RESULTS REPORT

I. INTRODUCTION

This document describes the application and experimental results associated with the Passive and Advanced Vibro-Acoustic Treatments Demonstration conducted at the Laboratory for Structural Acoustics, Naval Research Lab (NRL) during the winter and spring of 2001-2002. The goal of the demonstration is to utilize the most advanced treatments developed in the first part of the program (PAVAD-A), improve their design, and apply them to the sponsor supplied structure. In the initial PAVAD-A study, advanced treatments were applied to an idealized simple supported plate (test fixture apparatus) to evaluate the noise reduction performance and optimize the treatment designs. The design methodology and experimental results for PAVAD-A were previously reported^{1,2}. The basic design methodology and the associated control mechanisms for PAVAD-B can be found in these PAVAD-A documents since the fundamental approach is repeated here. Nearfield Acoustic Holography (NAH) measurements of the untreated sponsor supplied structure were also made and reported³. These data illustrate the structural response and provide a means to determine the optimized treatment locations. The performance of the improved PAVAD-B advanced treatments is evaluated using these same NAH techniques and reported in this document.

Control Technique	Performance	Cost	Weight	Reliability	Voltage
CLD, Partial	B	A	B	A	A
CLD, Complete	A	A-	C	A	A
ACLD	A	C	A	B	C
Modal Restructure	A	C	B	C	B
Piezo-dissipative	D	C	B	B	A
Tuner Absorber	D	B	D	B	A

Fig. 1 — Summary of results in PAVAD-A

II. BRIEF REVIEW OF PAVAD-A

The PAVAD-A advanced treatments were evaluated using NAH measurement techniques and the results are shown in Fig. 1. High performance is considered to be the most important evaluation criteria for this study. The “Advanced” Constrained Layer Damping (ACLD) and Modal Restructuring (MR) techniques demonstrated the highest levels of performance along with the complete coverage Constrained Layer Damping (CLD) treatment. The partial CLD treatment follows in a close second place with some limitations at very low frequency. The Piezo Dissipative (PD) and Tuned Vibration Absorber (TVA) are significantly behind with only very small levels of performance. In terms of cost, the advanced (system-on) treatments receive a poor grade because of the expense related to the actuators. The CLD treatments are of very low cost and receive the highest grades in this category. ACLD is the lightest weight system with modal

restructuring, partial CLD and complete CLD techniques being significantly heavier. The completely passive CLD systems are the most reliable, and ACLD also receives a good grade with its failsafe passive damping feature. The voltage levels associated with ACLD design are the highest in the 50-300 volt range, whereas, the MR system is considerably lower in the 15-130 volt range. Higher voltages are considered a safety issue. The CLD approaches do not require any power source and receive the highest grades in this category.

The PAVAD-B study will examine only the ACLD and MR advanced treatments since they displayed the most promise in terms of noise reduction performance. The CLD treatment has been dropped in PAVAD-B since the level of performance of this benchmark technique is understood and little improvement can be made to the design. Further, it is important to note that the passive component of the new ACLD design is very close to an optimum CLD design using RKU analysis. This ACLD design could serve as a baseline passive configuration (partial CLD treatment) for comparison to system-on approaches.

There are two improvements that were made to the PAVAD-A treatment designs for PAVAD-B. The first area of improvement involves increasing the passive performance of ACLD while maintaining adequate system-on performance. This improvement can be achieved through a stiffer constraining layer (actuator material). A monolithic PZT wafer will meet this goal and also reduce the voltage requirement. The PZT has greater mass, but low mass is not a significant objective of this program. The second significant area of improvement involves more sophisticated system monitoring. An increased number of surface mounted accelerometers will improve the performance of the "system on" techniques. The spatial density of the sensor layout must sufficiently sample the modes/wavenumbers under control. The industry trend is to use higher sensor counts with lower cost devices. Although not fully developed, MEMS accelerometers will offer a low cost solution in the near future.

III. PAVAD-B EXPERIMENTAL CONFIGURATION

The ACLD and MR treatments individually cover a portion of the sponsor supplied structure's side surface on the third sub-panel down (Panel #3) from the top (Fig. 2). This coverage represents only ~2.3% of the total surface area. The ACLD treatment is applied on the left side and the MR treatment is on the right side of the structure. The basic panel dimensions, thicknesses, and edge conditions are identical on the left and right sides. The only differences are related to non-symmetric internal shelf structure, which will only minimally affect the boundary conditions of the sub-panels. The third sub-panel is slightly thicker (.12 inches) than the top two panels (.06 inch) that were used to model the test fixture apparatus in PAVAD-A. The third panel was chosen because (1) data is available for this drive condition from previous measurements³, (2) the thicker system is more challenging to control, and (3) it is a panel near the center of the global structure. The shaker locations and accelerometer arrays are also shown in Fig. 2. Each treated sub-panel is excited at the front top corner by a F3 Wilcoxon electromagnetic shaker and an accelerometer array consisting of (8) Endevco 2250a accelerometers is mounted on each side for wavenumber/mode sensing.

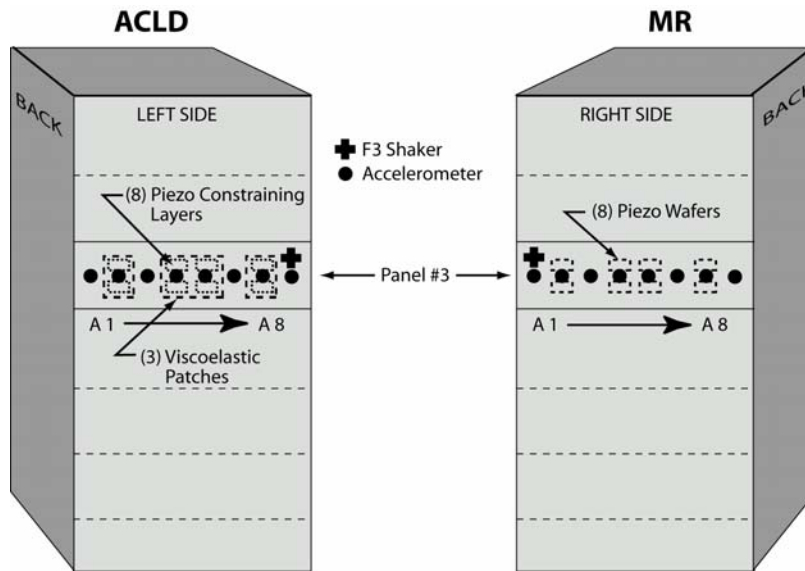


Fig. 2 — Advanced treatment locations and configuration of sponsor supplied structure in PAVAD-B

A. Nearfield Acoustic Holography (NAH) and Measurement Issues

The treatment evaluations were conducted using NAH measurements over the entire treated side of the structure. Both broadband and single frequency experiments were performed. The broadband measurements were used to characterize the system and evaluate the passive treatment. The single frequency measurements were conducted to fulfill the main requirement of the treatments evaluation, that is, to reduce the noise generated by low frequency tonal sources.

Broadband (10-3000 Hz) system characterization scans were performed with no treatment and with each treatment in the passive mode. The measurements had spatial sampling of 2.8 cm over a grid of 82 points (long dimension) and 46 points (short dimension). This grid produced an overall scan aperture of 2.3 m x 1.3 m, which includes an overscan region that is greater than 25 cm from the edge of the structure surface. The microphone standoff distance was 6 mm. The sampling rate of the data was 20 kHz, yielding a frequency resolution of 2.4 Hz.

Single mode frequencies below 700 Hz were chosen to evaluate the untreated, system-off (passive) and system-on configurations. The reduced bandwidth relaxes the spatial resolution requirement of the NAH scans. The spacing was reduced to 5.67 cm, yielding a grid of 41 points (long dimension) and 24 points (short dimension). The measurement aperture (2.3 m x 1.3 m), microphone standoff (6mm) and sampling of 20 kHz with 2.4 Hz resolution were chosen to be the same as the broadband case.

B. Advanced Treatment Design and Configuration

The ACLD and MR treatments are both applied internally to the sponsor supplied structure as illustrated in Fig. 2. The ACLD treatment design involves a .05 inch thick DYAD 601 viscoelastic layer cut into 3 patches, and the constraining layer/actuator consists of (8) .032

inch thick PZT4 monolithic wafers with the dimensions 2.75 inches x 2.0 inches. The goal of increasing the passive damping is more challenging since the base plate thickness has increased. Using the Ross-Kerwin-Ungar (RKU) analysis, the composite system in PAVAD-B represents a ~75% increase in damping from that in PAVAD-A. This increase is mainly due to a stiffer constraining layer, where the “Advanced” Fiber Composite (AFC) actuator used in PAVAD-A had a much lower stiffness. The MR treatment design involves the same (8) PZT-4 wafers applied to the opposite side of the structure in the same configuration as the ACLD, but without the viscoelastic layer.

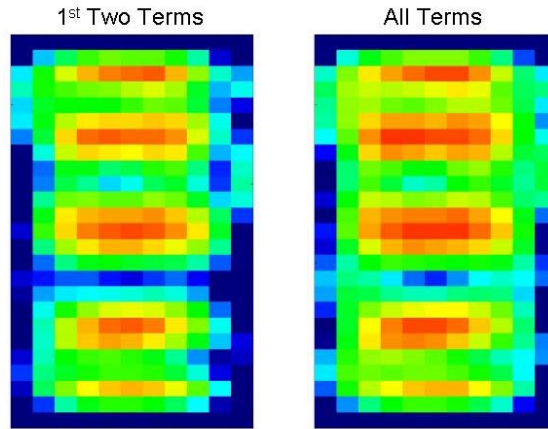


Fig. 3 — Summed strain energy from simply support plate in PAVAD-A

The ACLD and MR treatments were located on the panel in areas of high in-plane strain to maximize their control authority, and to increase the damping properties of the ACLD design. The strain energy due to bending and twisting for an isotropic plate may be represented as,

$$U = \frac{D}{2} \int_{Area} \left(\frac{\partial^2 w}{\partial x^2} \right)^2 + \left(\frac{\partial^2 w}{\partial y^2} \right)^2 + 2\nu \frac{\partial^2 w}{\partial x^2} \frac{\partial^2 w}{\partial y^2} + 2(1-\nu) \left(\frac{\partial^2 w}{\partial x \partial y} \right)^2, \quad (1)$$

where w is the normal velocity, D is the bending stiffness, ν is Poisson's ratio and the area is taken over x and y . See Appendix A for the derivation of the strain energy equation. The first three terms of Eq. 1 are associated with bending moments in the x - y plane. The last term is due to torsional moments associated with the twisting of the plate. This equation is a more precise representation of the strain energy than that found in¹. The cross terms have been included, but only have a minimal effect here due to the bending modes considered and lack of twisting motion. Fig. 3 shows the summed strain energy determined through spatial integration of the plate data from¹. The display shows the calculation using only the first 2 terms and all terms of Eq. 1. The conclusion in¹ concerning the treatment placement and use of the normal velocity to locate areas of high in-plane strain still holds and does not change. Displays of PAVAD-B normal velocity for each mode and the mode sums can be seen in Figs. 4 and 5 for the ACLD and MR treatments, respectively. The normalized mode sum (each individual mode normalized before sum) is used to place the treatments.

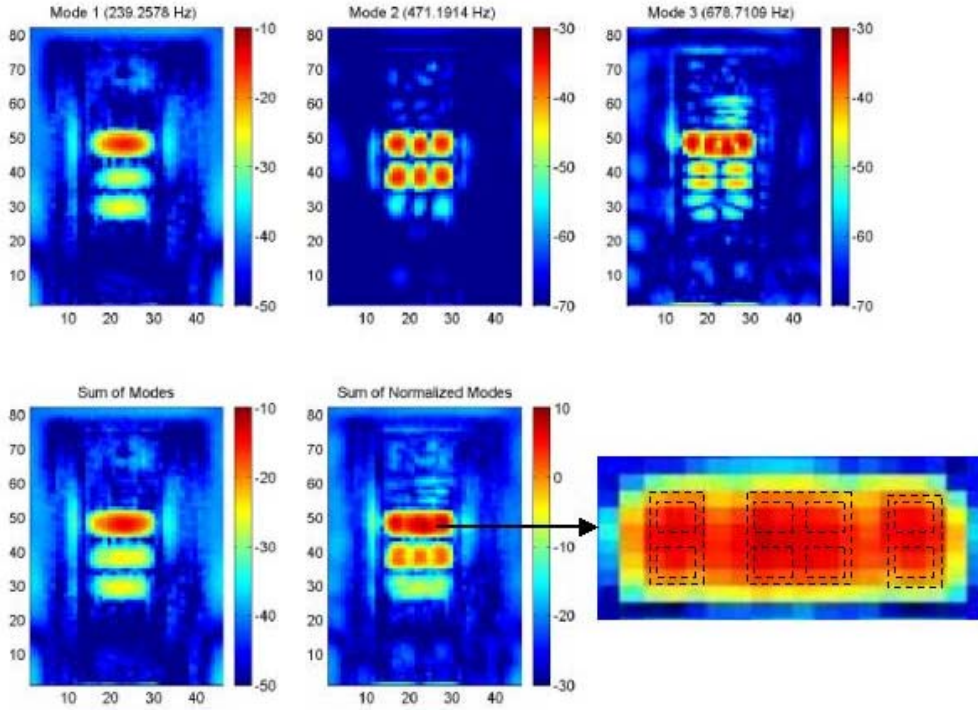


Fig. 4 — Individual modes and mode sum for ACLD treatment side on sponsor supplied structure. Exploded view of panel shows the optimized treatment location.

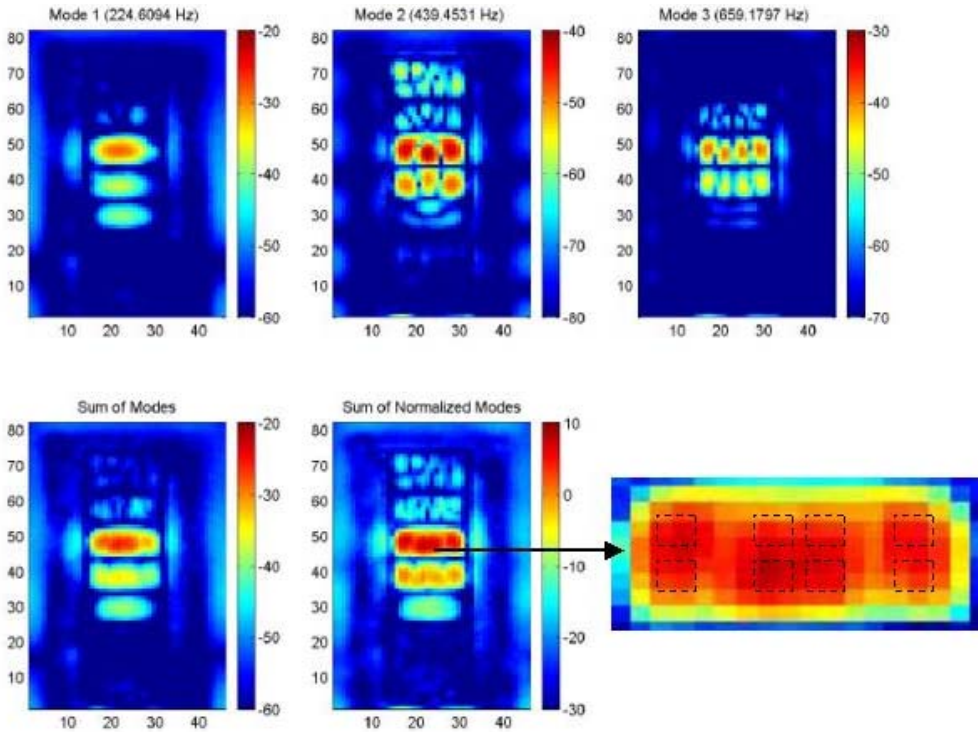


Fig. 5 — Individual modes and mode sum for MR treated side on sponsor supplied structure. Exploded view of panel shows the optimized treatment location.

The modes that will be targeted in the control experiments were selected by examining dominant peaks in the total farfield radiated power in the half space above the ACLD (Fig. 6) and MR (Fig. 7) treated structure sides. The input power normalization (Watts/Watt) represents the results in the most accurate fashion for comparison between the untreated and treated structures. The drive point impedance changes somewhat with the application of the treatment, and the use of force or velocity normalization will affect the performance evaluation results. The force normalized curves are shown as a reference.

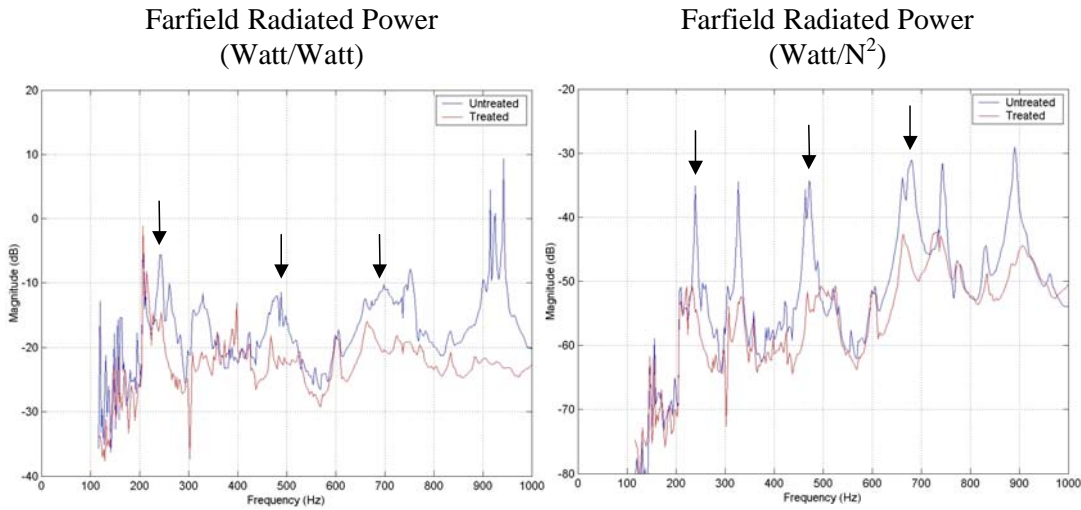


Fig. 6 — Total farfield radiated power normalized to input power and force for the half space over the ACLD side of sponsor supplied structure

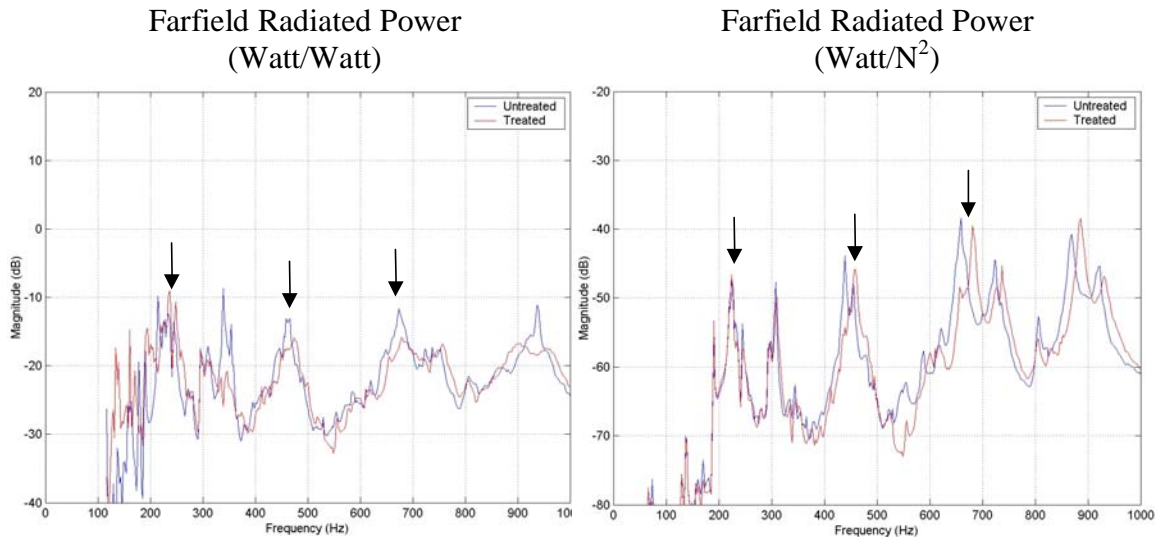


Fig. 7 — Total farfield radiated power normalized to input power and force for the half space over the MR treated side of sponsor supplied structure

The effect due to adding the treatment to structure can be observed by examining the drive point admittance shown in Fig. 8 for both the ACLD and MR treatments. The dominant

changes involve the addition of significant damping in the passive ACLD configuration, and a simple shift in mode frequencies due to the added composite stiffness in the MR case due to the PZT wafer. The MR mode frequencies shifted from 224.6, 439.5, and 659.2 Hz to 224.6, 459.0, and 681.2 Hz, respectively.

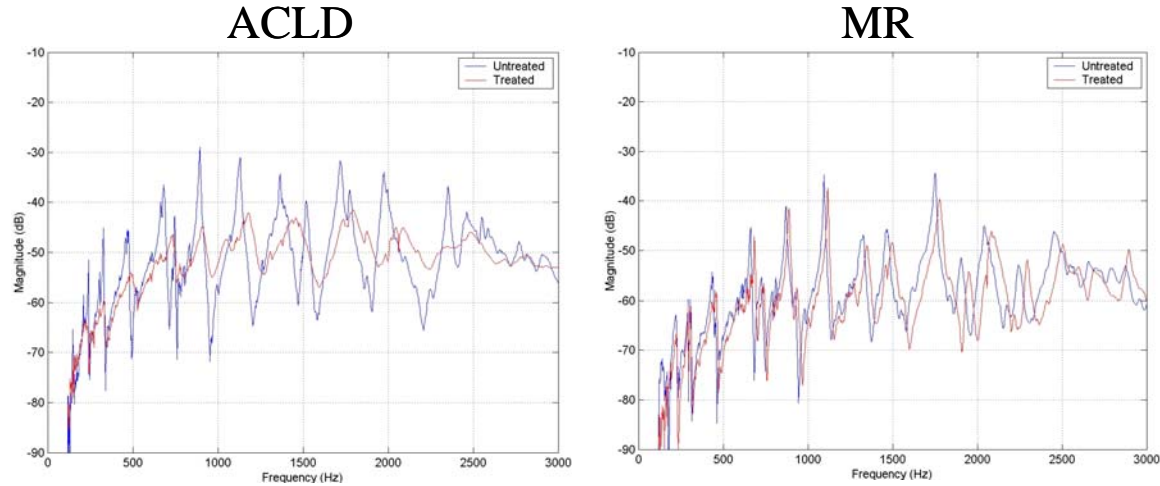


Fig. 8 — Drive point admittance comparison between untreated and treated surface of sponsor supplied structure

A comparison of drive point admittance for the ACLD systems in PAVAD-A (simply supported plate/panel) and PAVAD-B (structure sub-panel) can be seen in Fig. 9. The structural panel in PAVAD-B has a lower mode density below 500 Hz due to changes in panel thickness and boundary conditions. The PAVAD-B structure itself and the ACLD treatment each add more structural damping than the plate and ACLD treatment in PAVAD-A. The half power bandwidth method shows that the untreated structure in PAVAD-B has a .030 loss factor as compared to the .010 loss factor in the untreated PAVAD-A plate. It is common that structures with increased complexity have higher losses due to breaks in their structural symmetry and structural disorder. The PAVAD-B composite ACLD/structure has a loss factor of .116 as opposed to a .023 loss factor for the ACLD/plate in PAVAD-A. After removing the damping associated with their respective structures, these numbers represent an ~70% increase in damping of the PAVAD-B ACLD treatment when compared to the ACLD treatment design in PAVAD-A.

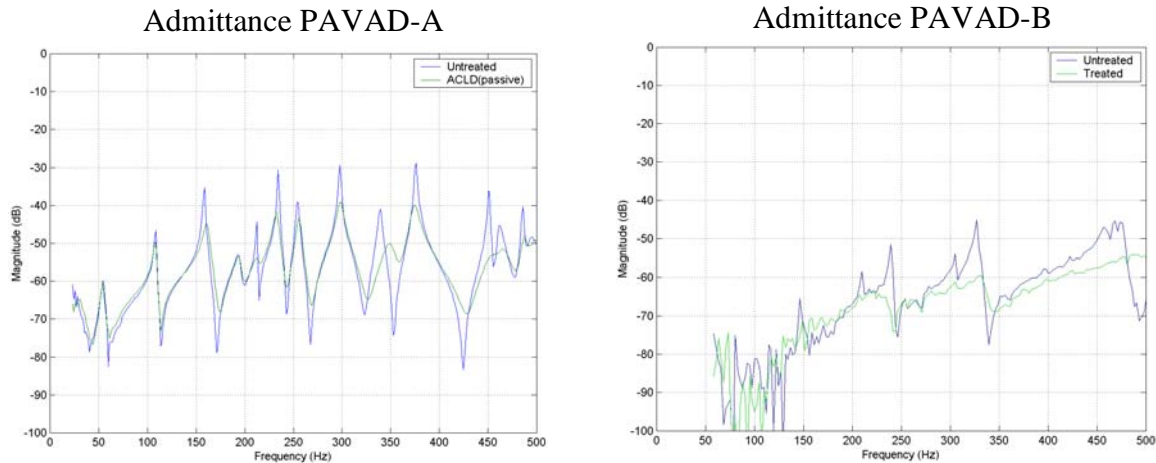


Fig. 9 — Drive point admittance comparison between ACLD treated surfaces in PAVAD-A and PAVAD-B

C. Control Laws and Configuration

The two fundamental feedforward control laws are point minimization of surface acceleration (illustrated in Fig. 10) near the center of panel #3 and point minimization of nearfield pressure (Fig. 11) at a distance of 40 centimeters from the center of the Panel #3 surface. Both control laws were implemented at each of the three chosen panel modes for ACLD and MR. Recall that these modes were chosen based on high levels of total farfield radiated power (see section B). The point acceleration controller minimized the A5 sensor for the ACLD experiments, and in the MR experiments, the A4 sensor was used. Both accelerometers are mounted slightly forward of the center of the panel. An off-center location was required to sense the (4,1) mode that has a vertical node line at the center.

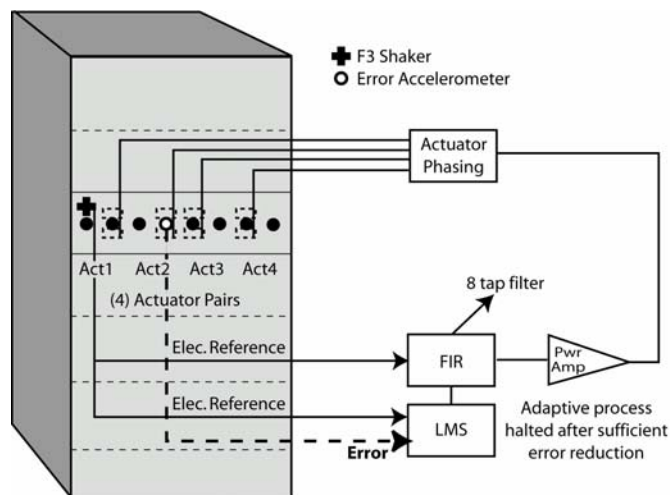


Fig. 10 — Control configuration for point minimization of surface acceleration

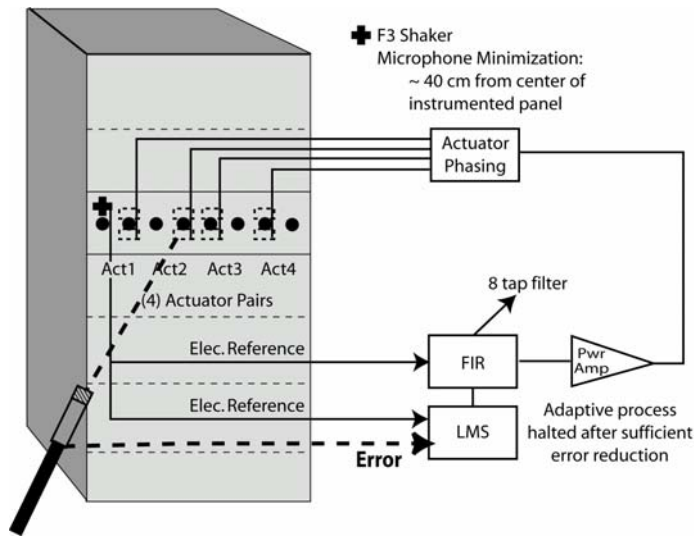


Fig. 11 — Control configuration for point minimization of pressure

The Single-Input Single-Output (SISO) FIR filter of the control configuration was formed via the use of an adaptive LMS (Least Mean Squared) algorithm. The two inputs to the LMS algorithm are an electrical reference that is correlated with the disturbance (F3 shaker) and the relevant error signal as prescribed by the control law. The LMS algorithm adapts eight weights in the FIR filter while the output drives a power amplifier and the treatment actuators. The adaptation occurs until the weights have converged and the error signal is minimized in a least mean squared sense. The number of weights (8) was found to be an optimum through experiment. This experimental process involved starting at a low number of weights and gradually increasing the number until no additional performance could be observed. Theoretically, only two weights are required to control a gain and phase at a single frequency, but in the presence of system noise and small system (plant) variations more weights are required. After convergence, the adaptation process is shut off, and the fixed FIR control filter performance is evaluated.

The additional flow block between the power amplifier and actuator in Figs. 10 and 11 illustrates the actuator phasing. The details of the actuator phasing are shown in Fig. 12. The red and green areas represent motion of the panel that is 180 degrees out-of-phase. Therefore, the actuator pairs are wired up differently depending on the mode type so that the proper control authority can be achieved. For example, all the actuator pairs are driven together for the (1,1) mode. For the (3,1) mode, the two vertical pairs in the center are driven out-of-phase with the outer two pairs, and the vertical pairs are driven with alternating phase for the (4,1) mode.

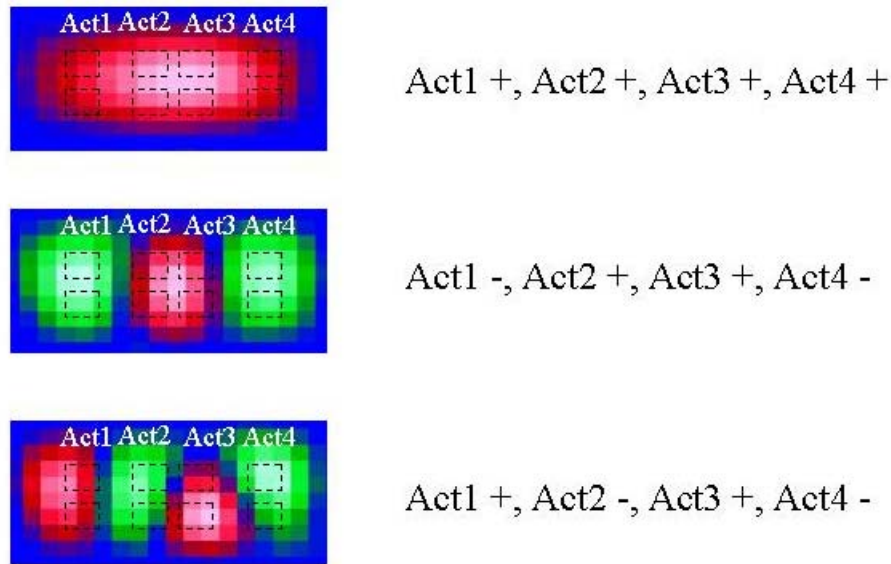


Fig. 12 — Actuator phasing for individual modes

A third control law was implemented using the modal sensing distribution of the accelerometer array to reduce the acoustic radiation of the (3,1) mode in the MR configuration. Figure 13 shows the configuration that involves the implementation of three independent SISOs loops. Each loop consists of its own error sensor, LMS algorithm, FIR filter, power amplifier and actuator. In a simultaneous manner, actuator pair #1 minimizes accelerometer A2, actuator pairs #2/#3 work to minimize accelerometer A4 and actuator pair #4 minimizes accelerometer A7 to provide the additional system performance.

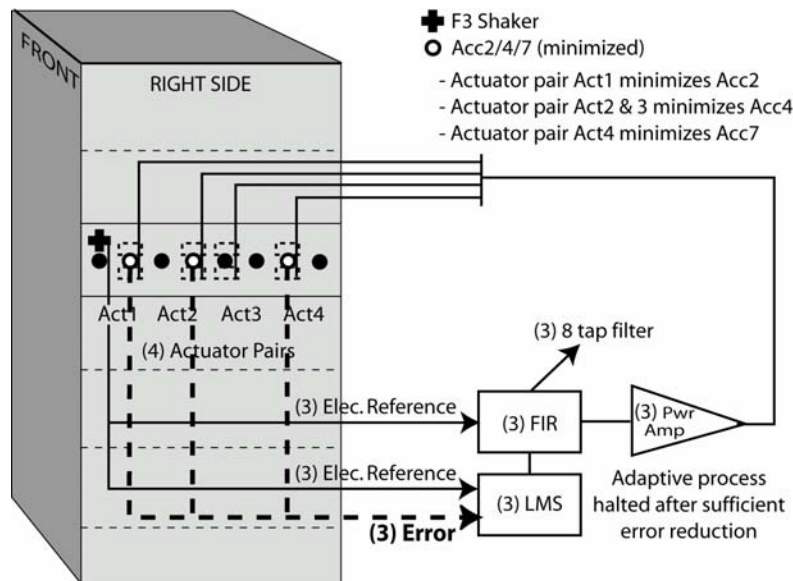


Fig. 13 — Multi-SISO configuration for minimization of surface acceleration

IV. ADVANCED TREATMENTS PERFORMANCE

The performance of the treatments is evaluated using two measurement approaches. First, the broadband passive effect of simply adding the treatment to the structure is examined. The treatment has the effect of adding, in varying degrees, mass, stiffness and damping to the structure. Detailed comparisons are made between the untreated and treated structure with this data. The second measurement set is used to evaluate the system-on performance of the panel at the selected tonal mode frequencies. Three low frequency modes are chosen that strongly contribute to the total farfield radiated power. Detailed evaluations are made between the untreated structure, treated structure (system-off) and system-on configurations.

A. Broadband Untreated/Treated (System-Off) Performance

The passive performance is evaluated by a metric using total farfield radiated power in the half space above the treated panel. The results are shown for both of the treatments in terms of units of (Watt/Watt) and (Watt/N²) in Figs. 14 and 15, respectively. The broadband curves are displayed from 100 to 3000 Hz. The passive ACLD treatment adds damping to the structure that becomes more significant as the frequency increases. A second order effect involves adding mass and stiffness that only slightly shifts the mode frequencies. In the case of MR, the direct attachment of the piezo wafer to the structure mostly adds stiffness to the structure, which has the effect of shifting modes to higher frequencies. Little additional damping of modes is observed with MR.

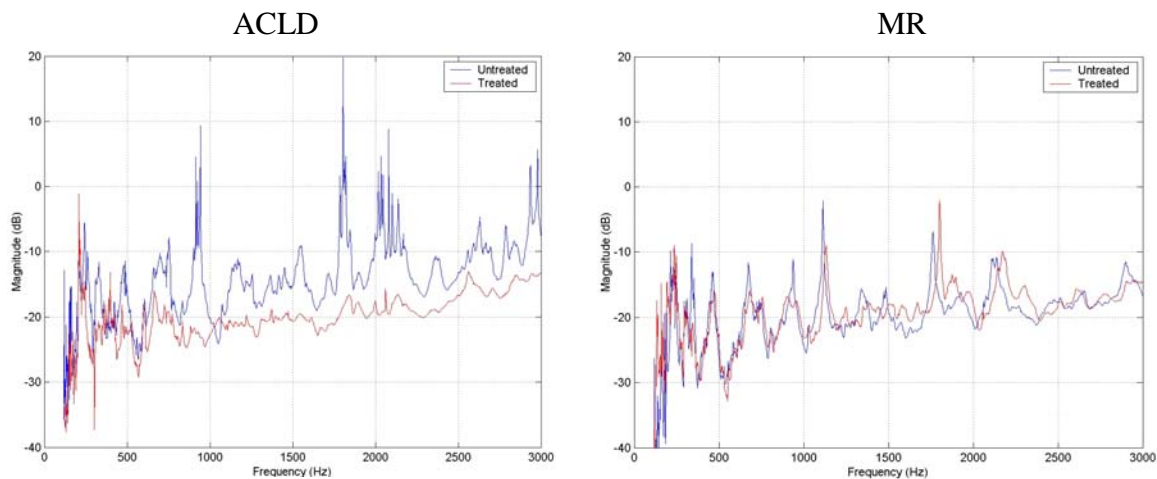


Fig. 14 — Total farfield power (Watts/Watt) in half space comparison of untreated and treated (passive) sponsor supplied structure

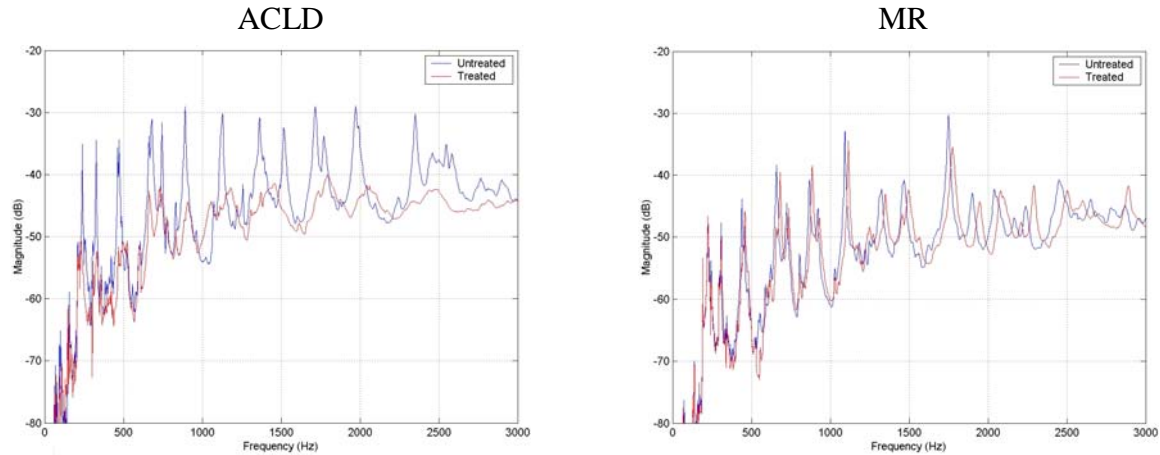


Fig. 15 — Total farfield power (Watts/ N^2) in half space comparison of untreated and treated (passive) sponsor supplied structure

The spatial distribution of normal surface velocity with and without treatment can be seen in Figs. 16 and 17 for the ACLD and MR treatments, respectively. The white lines indicate the outline of the cabinet side. Note that the ACLD color scales are different between the untreated and treated (system-off) cases, and that there is a 10-20 dB level reduction due the passive treatment alone. Also observe that Mode 3 has restructured on panel #3 from the (4,1) mode to a mode similar to a (1,2) mode. The (1,2) mode will become an issue since it has a node along the structure panel that coincides with the accelerometer array. The MR modes have for the most part maintained their mode shape, but modes 2 and 3 have shifted up in frequency.

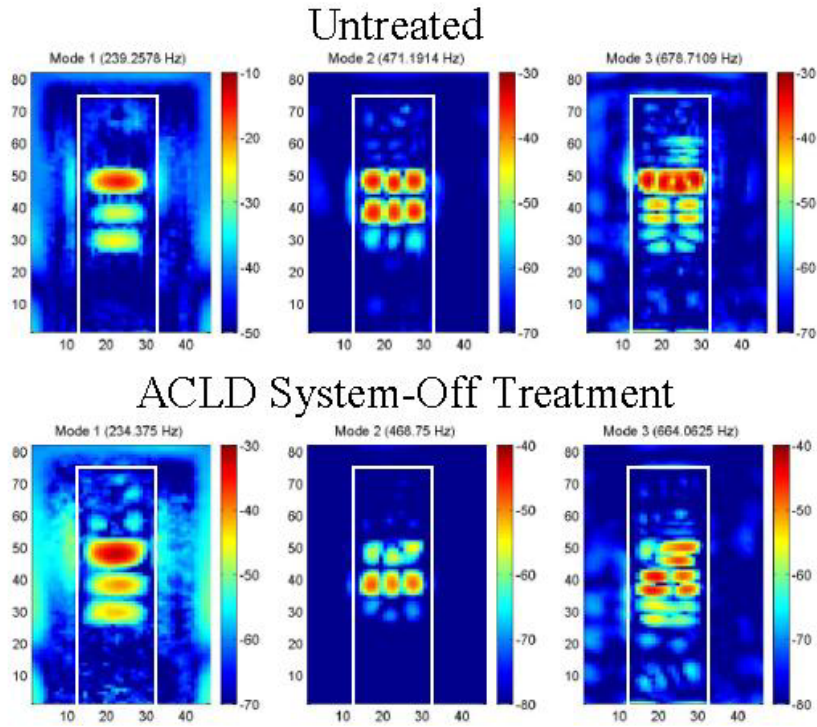


Fig. 16 — Spatial mode distribution for untreated and treated ACLD surface of sponsor supplied structure in PAVAD-B

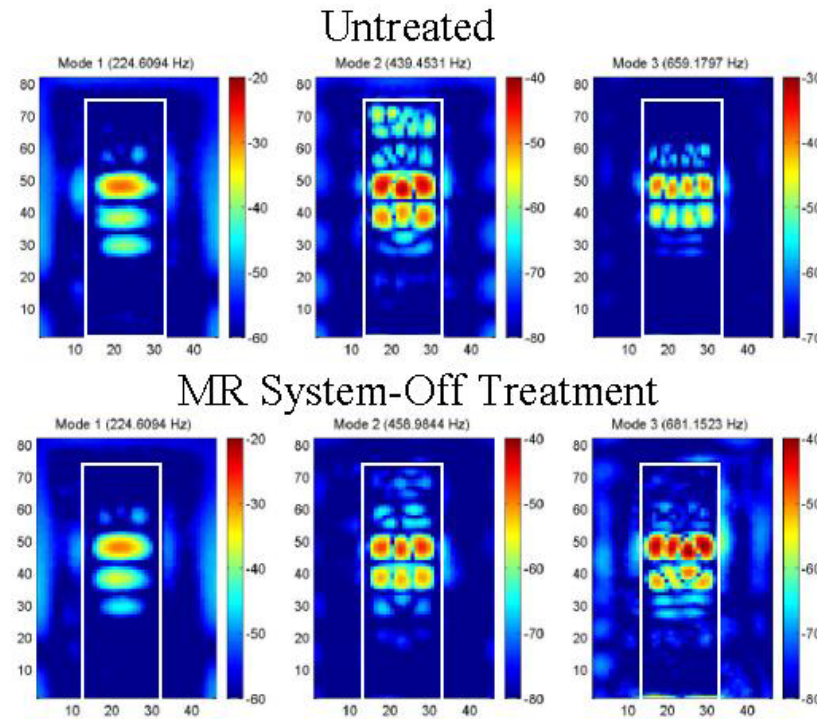


Fig. 17 — Spatial mode distribution for untreated and treated MR surfaces of sponsor supplied structure in PAVAD-B

B. Tonal Untreated/Treated(System-Off)/Treated(System-On) Performance

A typical example of a tonal control experiment is shown in Fig. 18. The display shows the response minimization of the A5 accelerometer for the ACLD mode #1 configuration. The point acceleration at 234 Hz is reduced by ~ 60 dB by the system-on control. The 1st and 2nd harmonics are excited due to small amounts (50 dB down) of harmonic distortion in the disturbance shaker source. The controller additionally treats the harmonic distortion by reducing the 1st harmonic by ~ 10 dB. Note that no harmonic distortion was added to the system by the control actuator.

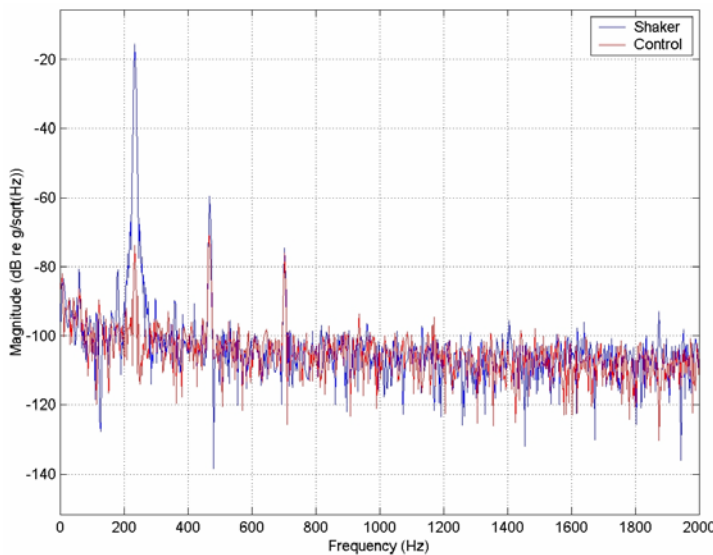


Fig. 18 — Typical reduction of error sensor during control experiment

Figures 19 through 24 illustrate the performance of both ACLD and MR single frequency control experiments. Bar graphs at the top of the figure illustrate the level of total farfield radiated power reduction due to the passive system-off and system-on configurations as compared to the untreated response. Note that the shift in the mode frequencies has been accounted for in these performance evaluations. The spatial distributions of surface velocity for the untreated, treated, and various control configurations are shown at the bottom of the figures. Note that these modal displays illustrate the phase of the mode. That is, a display of the real part of the response where each are normalized to the individual displays. These display are not for the purpose of observing attenuation, but simply to view the spatial distribution of the surface velocity.

Figures 19, 20 and 21 show the performance for the three modes examine under ACLD control. Performance at modes 1 and 2 showed that system-off ACLD treatment reduced the total farfield power by ~ 8 dB and system-on configurations added another 5 to 18 dB, yielding a 13 to 25 dB total reduction in farfield radiated power. On the surface, the normal velocity levels are attenuated, but modal restructuring is also responsible for some of the farfield performance in the ACLD control cases. The (1,1) mode is split into a (2,1) mode, and the (3,1) mode changed to something resembling a (4,1) mode. The third mode proved to be unobservable because the mode shape had changed (due to addition of treatment) such that a node existed at the accelerometer sensor locations.

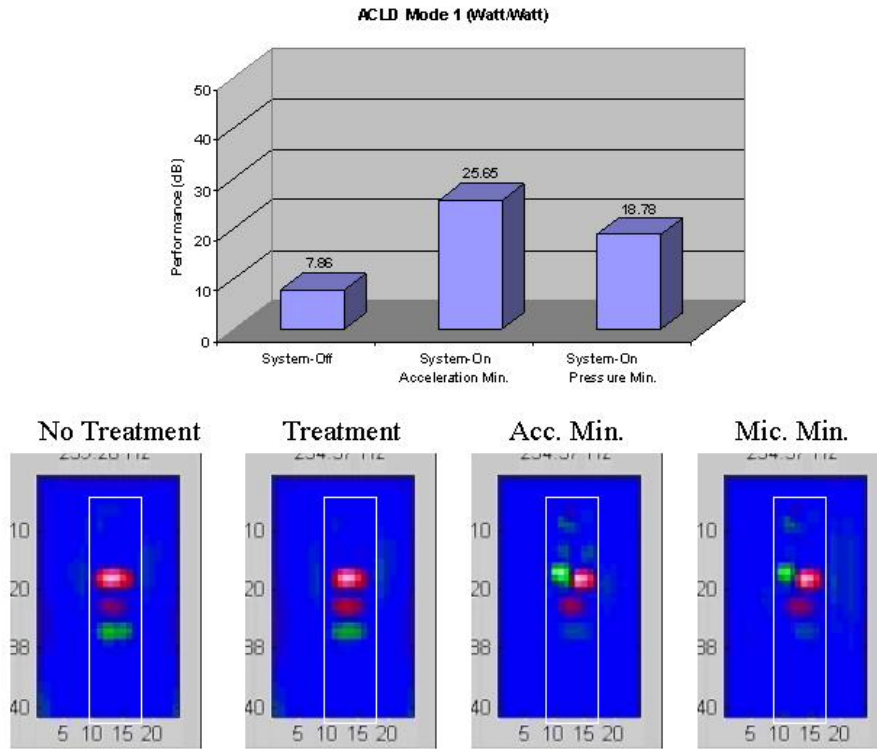


Fig. 19 — ACLD mode #1 performance results on sponsor supplied structure in PAVAD-B

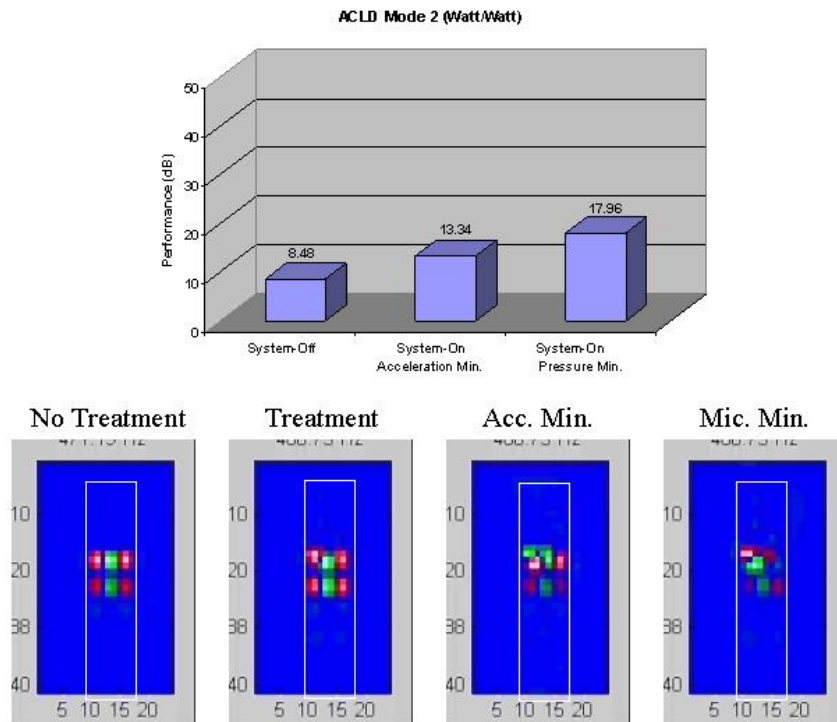


Fig. 20 — ACLD mode #2 performance results on sponsor supplied structure

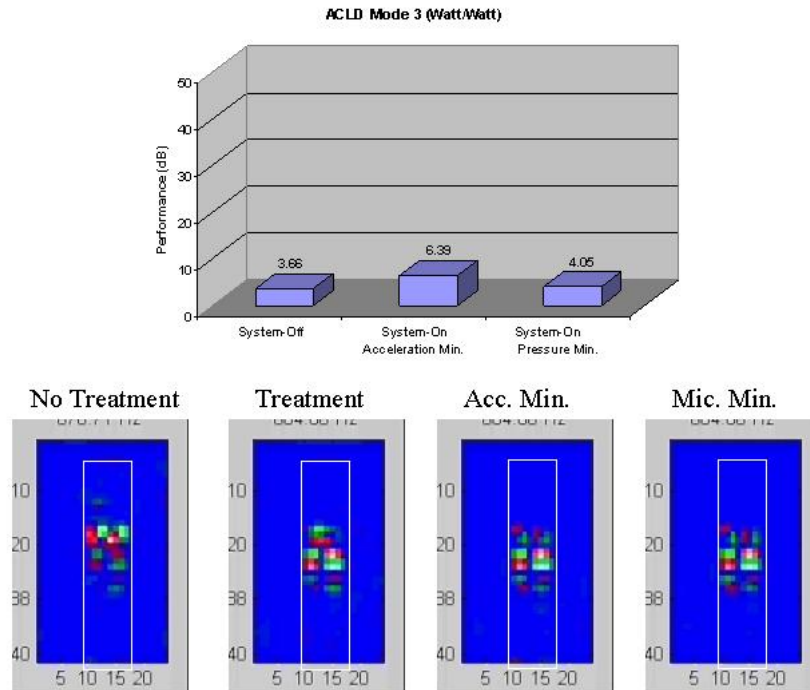


Fig. 21 — ACLD mode #3 performance results on sponsor supplied structure

MR control performance for the three modes is illustrated in Figs. 22, 23 and 24. The farfield showed little reductions due to the simple addition of the treatment (0-3 dB). Recall that the effect of the treatment mostly adds mass and stiffness to the structure, slightly shifting the mode frequencies. The range of system-on MR performance under single SISO control showed an additional 2 to 13 dB for the various modes. The total performance for single SISO control was 3 to 15 dB.

Multi-SISO control of the second MR mode (3,1) showed superior performance with a total of 40 dB of reduction in the total farfield radiated power (Fig. 23). Magnitude displays for the MR mode 2 (3,1) experiments are shown in Fig. 25. Significant global reduction of the normal surface velocity is achieved in the multi-SISO case using accelerometers A2, A4 and A7, and no clear modal structure is observed. The Multi-SISO controller was found to be stable, but the adaptation of the separate loops showed higher levels of fluctuations during convergence of the three control filters. The separate controllers respond to the changes in the each other's control loops until each controller has learned something about the other's response and the symbiotic goal of reducing all of the three error signals is reached.

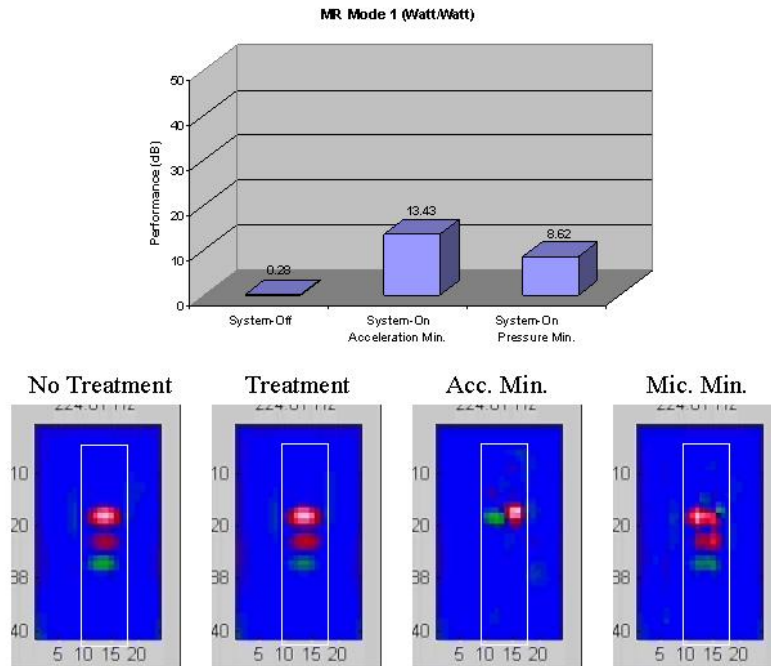


Fig. 22 — MR mode #1 performance results on sponsor supplied structure

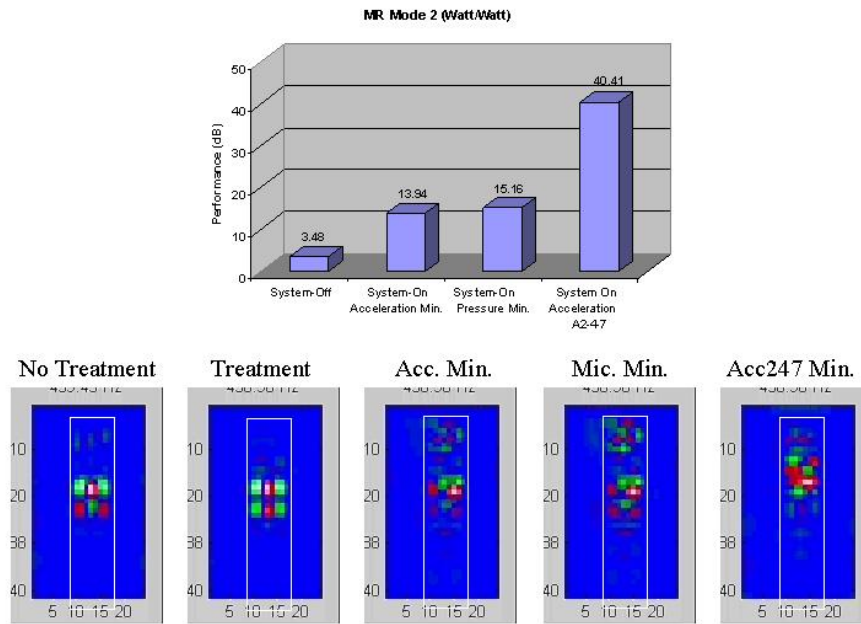


Fig. 23 — MR mode #2 performance results on sponsor supplied structure

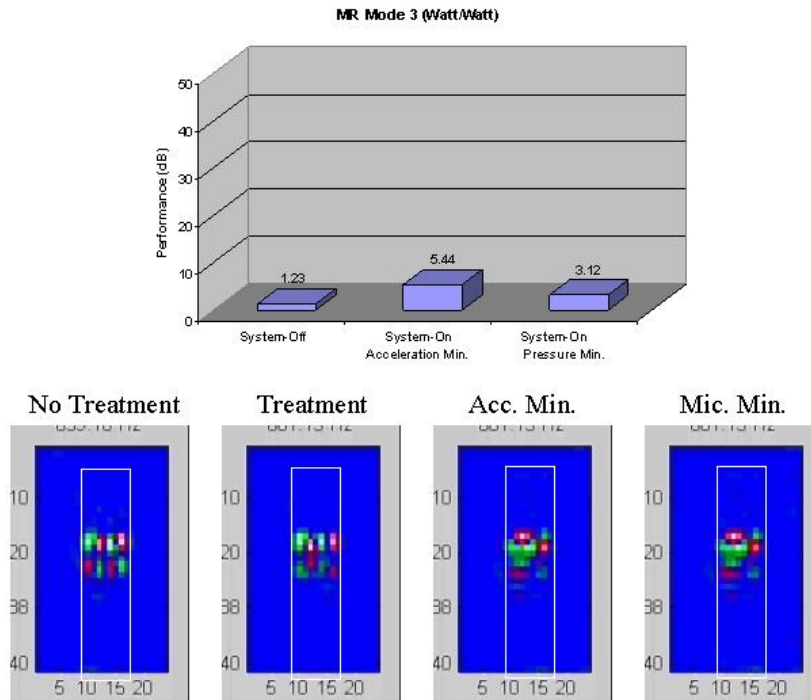


Fig. 24 — MR mode #3 performance results on sponsor supplied structure

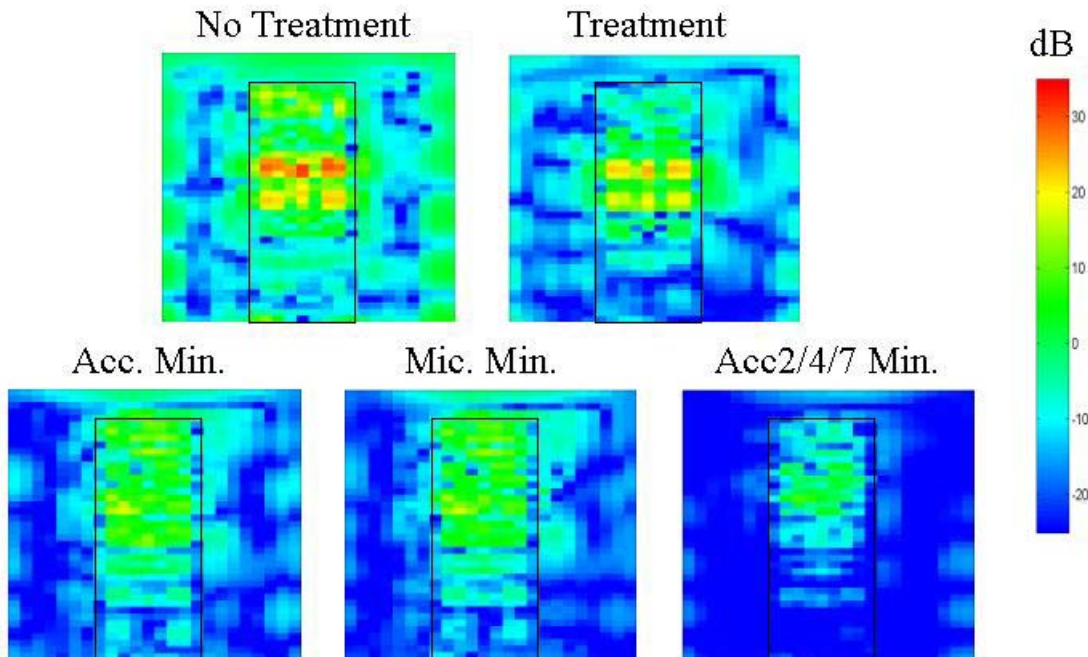


Fig. 25 — Magnitude displays that illustrate the surface velocity reduction on the sponsor supplied structure under MR control (mode #2). Note the strong attenuation of the multi-SISO control configuration (Acc2/4/7 Min.) and lack of low order radiating modes

The voltage requirement from these SISO control experiments is 38-60 volts for ACLD and 4-9 Volts for MR. The voltages are considerable less than were found in PAVAD-A due to the use of the PZT-4 actuator material in the design. A trade off in the multi-SISO case involves increasing the voltage to 40 volts in order to obtain an additional 25 dB increase in performance.

V. CONCLUSIONS

ACLD and MR treatments in PAVAD-B showed good to excellent performance. The nominal reduction of total farfield radiated power in the half space for the ACLD and MR treatments in the SISO configuration was 13-25 dB and 9-15 dB, respectively. The increased performance level found in ACLD over MR (~3-10 dB) may be accounted for by the hybrid nature of the technique. If the passive performance of ACLD were removed, then both treatments would show approximately the same level of reduction in terms of the farfield radiated power.

The PAVAD-B reduction levels are lower than that achieved in PAVAD-A by about 20-40 dB, but it should be realized that the percentage of surface area coverage was also greatly reduced. Recall that the PAVAD-B treatments only covered 2-3% of the total side area of the structure as compared to ~30% plate coverage in PAVAD-A.

Superior performance was found using a Multi-SISO configuration. A total reduction of ~40dB was found when examining the second MR mode. The Multi-SISO configuration is formed by three surface mounted accelerometers used for modal sensing, and breaking out three actuators from the larger actuator used in the single SISO experiments. It is important to recognize that the Multi-SISO configuration is still relatively simple in that full interconnectivity between all sensors and actuators through the processor is not required.

The modification of the PAVAD-A system proved fruitful in PAVAD-B. ACLD passive damping levels were increased by ~70% through the addition of a stiffer piezoceramic constraining layer. The PZT-4 material used as the ACLD actuator also reduced the required voltage to less than 60 Volts as oppose to several hundred volts in the PAVAD-A system. The PZT-4 material has higher actuator authority than the Active Fiber Composite used in PAVAD-A ACLD treatment design. The SISO MR voltage levels were even less, below 8 Volts. The Multi-SISO case demonstrated a trade-off between performance and voltage. Total performance was increase by 25 dB at the expense of increasing drive levels to 40 Volts. These voltage levels are all considered relatively low and safe for operation.

REFERENCES:

1. Peter C. Herdic, Robert D. Corsaro and Brian H. Houston, "PAVAD-A Part I: Design Document", NRL/MR/7130--01-8511.
2. Peter C. Herdic, Brian H. Houston, Robert D. Corsaro and Larry Kraus, "PAVAD-A Part II: Final Design and Experimental Results", NRL/MR7130--02-8652.
3. Peter C. Herdic, Earl G. Williams, Brian H. Houston, Robert D. Corsaro and Larry Kraus, "Nearfield Acoustic Holography Measurements of an Equipment Enclosure", NRL/MR/7130--02-8528.

APPENDIX A

The strain energy in an elastic 3-dimensional body,

$$U = \frac{1}{2} \int_{Volume} \sigma_x \varepsilon_x + \sigma_y \varepsilon_y + \sigma_z \varepsilon_z + \tau_{xy} \gamma_{xy} + \tau_{yz} \gamma_{yz} + \tau_{zx} \gamma_{zx}. \quad (\text{A.1})$$

The transverse stresses in a plate are small, therefore,

$$\sigma_z = \tau_{yz} = \tau_{zx} = 0, \quad (\text{A.2})$$

The strains and stresses due to bending and torsional moments for an isotropic plate,

$$\varepsilon_x = -z \frac{\partial^2 w}{\partial x^2}, \quad \varepsilon_y = -z \frac{\partial^2 w}{\partial y^2}, \quad \gamma_{xy} = -2z \frac{\partial^2 w}{\partial x \partial y} \quad (\text{A.3})$$

$$\sigma_x = \frac{E(\varepsilon_x + \nu \varepsilon_y)}{1 - \nu^2}, \quad \sigma_y = \frac{E(\varepsilon_y + \nu \varepsilon_x)}{1 - \nu^2}, \quad \tau_{xy} = G \gamma_{xy}, \quad G = \frac{E}{2(1 + \nu)}. \quad (\text{A.4})$$

Direct substitution of A.2, A.3 and A.4 into A.1, and integrating over thickness yields the strain energy in an isotropic plate for bending and torsional moments,

$$U = \frac{1}{2} \int_{Area} \left[\frac{E \left[\left(\frac{\partial^2 w}{\partial x^2} \right)^2 + \left(\frac{\partial^2 w}{\partial y^2} \right)^2 + 2\nu \left(\frac{\partial^2 w}{\partial x^2} \frac{\partial^2 w}{\partial y^2} \right) \right]}{1 - \nu^2} + \frac{2E \left(\frac{\partial^2 w}{\partial x \partial y} \right)^2}{1 + \nu} \right] \frac{z^3}{3} \Bigg|_{-h/2}^{h/2} \quad (\text{A.5})$$

After evaluation from $h/2$ to $-h/2$ and multiplying the last term by $\frac{1-\nu}{1-\nu}$ yields,

$$U = \frac{D}{2} \int_{Area} \left(\frac{\partial^2 w}{\partial x^2} \right)^2 + \left(\frac{\partial^2 w}{\partial y^2} \right)^2 + 2\nu \frac{\partial^2 w}{\partial x^2} \frac{\partial^2 w}{\partial y^2} + 2(1-\nu) \left(\frac{\partial^2 w}{\partial x \partial y} \right)^2 \quad (\text{A.6})$$

where,

$$D = \frac{Eh^3}{12(1-\nu^2)}. \quad (\text{A.7})$$